

SUPPLEMENTARY ONLINE MATERIALS

for

Unique localization of the plastid specific ribosomal proteins in the chloroplast ribosome small subunit provides mechanistic insights into the chloroplastic translation

Tofayel Ahmed¹, Jian Shi² and Shashi Bhushan^{1,3,*}

¹School of Biological Sciences, Nanyang Technological University, Singapore

²Center for BioImaging Sciences, National University of Singapore, Singapore

³NTU Institute of Structural Biology, Nanyang Technological University, Singapore

* To whom correspondence should be addressed. Tel: +65 6592 3673; Fax: +65 6791 3856;

E-mail: sbhushan@ntu.edu.sg

Figure S1: Purification of the chloroplast 70S ribosome and estimation of local resolution.

(a) Purification of the chloroplast 70S ribosome through sucrose density gradient centrifugation. Absorbance was measured at 280 nm and is represented by the red curve. Fractions corresponding to 70S chloroplast ribosomes were pooled (dotted lined box). **(b)** Representative micrograph collected at -2.9 μm defocus showing distribution of chloroplast ribosome particles. **(c)** Examples of representative 2D classes denoting a mixture of 50S and 70S chloroplast ribosome particles in the dataset. **(d)** Local resolution estimation using ResMap (1). Solvent exposed and sliced views are presented showing better resolved density at the core of the EM reconstructions while peripheral regions show relatively poor-resolved density. **(e)** Refinement validation. Red: Fourier Shell Correlation (FSC) curves are displayed for the 70S, 50S and 30S EM reconstructions with estimated resolution of 3.36 \AA , 3.3 \AA and 3.73 \AA , respectively (FSC=0.143 criterion) (2). Black: FSC curves generated from the final cryo-EM maps and maps derived from the refined atomic coordinates; FSC=0.5 criterion was used to report resolution.

Figure S2: Cryo-EM data processing. **(a)** From 3161 micrographs collected, 1285 turned out to be of good quality possessing minimal drift and no astigmatism. From these 1285 micrographs, 188K particles were semi-automatically picked using e2boxer.py of EMAN 2.1 (3). Data was processed using RELION 1.4 (4). 2X-binned particles were sorted using 2D classification generating 133K good particles which were subjected to 3D classification using a chloroplast ribosome 70S map as reference (5). 3D classification sorted out the bad and the 50S particles from the dataset. To reconstruct high-resolution maps of the 70S ribosome, 81K good 70S particles were refined using unbinned particles, generating a 3.66 \AA -resolved 70S map which yielded a 3.36 \AA -resolved map after inclusion of the movie frames in subsequent 3D refinement steps. Application of masks on the ribosomal subunits rendered maps of the LSU at

3.3 Å and of the SSU at 3.7 Å. **(b)** Molecular surface representation of the LSU model, built in our 3.3 Å map, based on our earlier LSU structure (5). Constituent proteins and rRNAs are indicated. Models for uL1c, uL10c, uL11c and bL12c could not be generated due to flexibility.

Figure S3: Local agreement between cryo-EM map and model. The final 70S, 50S and 30S cryo-EM maps of chloroplast ribosome coloured based on local correlation values between the final cryo-EM maps and the maps derived from atomic coordinates.

Figure S4: Representative density displaying map quality. **(a)** Representative density from 3.3 Å LSU map showing a 23S rRNA region surrounding G2379 (denoted by a star), interacting with protein bL35c (in green). **(b)** Representative density from 3.7 Å SSU map showing a 16S rRNA region surrounding U1137 (denoted by a star), interacting with protein uS3c (in pink).

Figure S5: Constituent proteins of the chloroplast ribosome SSU. Isolated densities for the chloroplast ribosome SSU proteins are in blue meshes with fitted models in dark red (left). The chloroplast SSU protein models overlaid with the corresponding homologous *E. coli* protein models (6) in grey for comparison. Density for cS22 is filtered to 8 Å for better visualization of the connecting density between the two RNA recognition motif (RRM) domains. Plastid specific protein extensions are colored in green.

Figure S6: mRNA entry site **(a)** The overall architecture of the mRNA entry sites in ribosomes from bacteria (PDB ID: 4YBB) (6), chloroplast and mitochondria (PDB ID: 5AJ3) (7) are compared to show unique features. rRNAs are in grey spheres. The structural landmarks of the ribosome are indicated. **(b)** Zoomed-in view of the mRNA entry sites from all three ribosomes (SSU) displayed in (a). The mRNA entry sites are marked with asterisks and the proteins in close

vicinity are displayed. Compared to bacteria, mRNA entry site in chloroplast ribosome appears to be constricted due to the presence of N-terminal extension in uS5c.

Figure S7: cS23 localizes to the mRNA exit site and comparison between the mRNA exit sites of bacterial, chloroplastic and mitochondrial ribosomes (a) *T. thermophilus* ribosome SSU from PDB ID: 4V6F (8) (grey) overlaid with chloroplast ribosome SSU displaying localization of cS23 closer to the site of SD-anti SD interaction in bacterial ribosomes (b) The overall architecture of the mRNA exit sites in bacterial (PDB ID: 4YBB) (6), chloroplast and mitochondrial (PDB ID: 5AJ3) (7) ribosomes are compared to show unique features. rRNAs are rendered in grey atoms. Proteins are colored golden rod, except for those that contribute in the formation of the mRNA exit sites. (c) Zoomed-in view of the mRNA exit sites from all three ribosomes depicted in (b). The mRNA exit sites are marked with asterisks and the proteins in close vicinity are displayed. Unique localization of cS23 at the mRNA exit site of the chloroplast ribosome makes the site narrower compared to bacteria.

Figure S8: Plastid pY is homologous to bacterial cold shock protein pY (a) Model of plastid pY (NTD) overlaid with *E. coli* cold shock protein pY (PDB ID: 4Y4O) (9) to show the presence of an extra loop between $\beta 2$ and $\beta 3$ in plastid pY. (b) Global sequence alignment between plastid pY and bacterial pY using EMBOSS Needle online server (10). Due to the presence of C-terminal extension for which we didn't observe any density, plastid pY is doubled in length than bacterial pY.

Figure S9: Conserved intersubunit bridges of the chloroplast 70S ribosome. Most of the intersubunit bridges are conserved in chloroplast ribosomes compared to bacterial ribosomes except for B7b which is absent from the chloroplast ribosome. Absence of B7b is replaced by the novel bridge B7c (refer main text, Fig. 6). Although, protein-protein (b), protein-rRNA (a, c, g,

h, j and l) and rRNA-rRNA (d, e, f, i and k) interactions contribute in the formation of the bridges, rRNA-rRNA type of interactions are the predominant types. The densities for the individual bridges are isolated and are shown in transparent surface (grey). The densities are low-pass filtered for better visualization.

Supplementary Table S1. Data collection and refinement statistics

Data Collection	70S ribosome	30S subunit	50S subunit
Particles	81305	81305	81305
Pixel Size (Å)	1.05	1.05	1.05
Defocus Range (μM)	0.4-3.7	0.4-3.7	0.4-3.7
Voltage (kV)	300	300	300
Electron Dose (e ⁻ Å ⁻²)	37.5	37.5	37.5

Model composition			
Non-hydrogen atoms	146,970	54,641	92,329
Protein residues	6,167	2,859	3308
RNA bases	4,496	1478	3018

Refinement			
Resolution (Å)	3.36	3.73	3.30
Map sharpening B-factor (Å ²)	-72.6	-97.9	-89.6
CC _{map model} (whole unit cell)	0.775	0.778	0.713

RMS deviation			
Bonds (Å)	0.01	0.02	0.01
Angles (°)	1.31	1.54	1.17

Validation (proteins)			
Molprobit score	2.59	2.86	2.16
Clashscore, all atoms	8.58	13.01	6.15
Poor rotamers (%)	1.26	1.54	1.02
Favoured rotamers (%)	94.78	94.95	94.63

Ramachandran plot			
Favored (%)	85.97	85.76	86.17
Outliers (%)	0.85	1.61	0.18

Validation (RNA)			
Correct sugar puckers (%)	99.78	99.80	99.77
Good backbone conformations (%)	77.48	78.56	76.95

Supplementary Table S2. Components of spinach chloroplast ribosome LSU model. The nomenclature of the ribosomal proteins is based on Ban *et al* (11).

Protein/RNA name	Old Name	Chain ID	Uniprot ID (GenBank ID)	Mature protein (range, aa)	Built residues (range, aa)	Size of homologous <i>E. coli</i> proteins (aa)	Comments
uL1c	RPL1		Q9LE95	73-352		234	Poor density, model could not be built
uL2c	RPL2	C	P06509	1-272	23-269	273	
uL3c	RPL3	D	(KNA04906.1)	85-305	86-297	209	
uL4c	RPL4	E	O49937	51-293	52-261	201	
uL5c	RPL5	F	(KNA19821.1)	39-258	56-230	179	
uL6c	RPL6	G	(KNA14466.1)	39-220	42-214	177	
bL9c	RPL9	H	(KNA21690.1)	42-196	43-95	149	
uL10c	RPL10	I	(KNA14105.1)	53-232		165	Poor density, model could not be built
uL11c	RPL11	J	P31164	67-224		142	Poor density, model could not be built
bL12c	RPL12		P02398	57-189		121	Poor density, model could not be built
uL13c	RPL13	K	P12629	54-250	54-246	142	
uL14c	RPL14	L	P09596	1-121	1-121	123	
uL15c	RPL15	M	(KNA06817.1)	80-271	80-256	144	
uL16c	RPL16	N	P17353	1-135	2-135	136	
bL17c	RPL17	O	(KNA19692.1)	11-126	11-126	127	
uL18c	RPL18	P	(KNA08833.1)	44-166	47-166	117	
bL19c	RPL19	Q	P82413	78-233	115-232	115	
bL20c	RPL20	R	P28803	1-128	3-117	118	
bL21c	RPL21	S	P24613	56-256	88-234	103	
uL22c	RPL22	T	P09594	1-199	26-169	110	
uL23c	RPL23	U	Q9LWB5	77-198	102-193	100	
uL24c	RPL24	V	P27683	47-191	50-173	104	
bL27c	RPL27	X	(KNA14420.1)	58-194	66-165	85	
bL28c	RPL28	Y	(KNA16864.1)	72-148	72-145	78	
uL29c	RPL29	Z	(KNA15596.1)	60-168	63-152	63	
bL31c	RPL31	0	(KNA12538.1)	37-130	38-101	70	Poor density
bL32c	RPL32	1	P28804	1-57	2-47	57	
bL33c	RPL33	2	P28805	1-66	9-59	55	
bL34c	RPL34	3	P82244	91-152	91-147	46	
bL35c	RPL35	4	P23326	87-159	89-157	65	
bL36c	RPL36	5	P12230	1-37	1-37	38	
cL37	PSRP5	6	P27684	63-142	94-142		

cL38	PSRP6	7	P82411	48-116	48-93		
23S rRNA		A	AJ400848.1	2810 nucleotides	1-2810		
5S rRNA		B	AJ400848.1	121 nucleotides	3-119		
4.8S rRNA		W	AJ400848.1	106 nucleotides	5-106		

Abbreviations: PSRP=Plastid-specific ribosomal proteins.

Supplementary Table S3. Components of spinach chloroplast ribosome SSU model. The nomenclature of the ribosomal proteins is based on Ban *et al* (11).

Protein/RNA name	Old Name	Chain ID	Uniprot ID (GenBank ID)	Mature protein (range, aa)	Built residues (range, aa)	Size of homologous <i>E. coli</i> proteins (aa)	Comments
bS1c	RPS1	8	P29344	370	49-74, 249-377	557	Poor density. N- and C-terminal extensions, and OB domain was rigid body fitted
uS2c	RPS2	b	P08242	236	5-231	241	
uS3c	RPS3	c	P09595	217	3-215	233	
uS4c	RPS4	d	P13788	200	2-197	206	
uS5c	RPS5	e	Q9ST69	253	138-308	167	
bS6c	RPS6	f	P82403	146	97-207	131	
uS7c	RPS7	g	P82129	154	4-152	179	
uS8c	RPS8	h	P09597	133	1-134	130	
uS9c	RPS9	i	P82278	157	63-195	130	
uS10c	RPS10	j	(KNA23234.1)	122	98-195	103	
uS11c	RPS11	k	P06506	137	21-138	129	
uS12c	RPS12	l	P62128	122	1-123	124	
uS13c	RPS13	m	P82163	126	32-141	118	
uS14c	RPS14	n	P06507	99	2-100	101	
uS15c	RPS15	o	Q9M314	90	21-82	89	
bS16c	RPS16	p	P28807	88	1-80	82	
uS17c	RPS17	q	(KNA21507.1)	108	58-135	84	
bS18c	RPS18	r	Q9M3K7	101	21-84	75	
uS19c	RPS19	s	P06508	91	7-84	92	
bS20c	RPS20	t	*	108	76-180	87	
bS21c	RPS21	u	KNA18384.1	137	95-138	71	
bTHXc	PSRP4	x	P47910	47			
cS22	PSRP2	v	P82277	198	71-260		Two RRM domains individually rigid body fitted. Helical linker was added thereafter
cS23	PSRP3	w	P82412	121	96-179		Core fold rigid body fitted
plastid pY	PSRP1	y	P19954	236	70-177	113	
16S rRNA		a	AJ400848.1	1491 nucleotides	1-1488		

Abbreviations: PSRP=Plastid-specific ribosomal proteins.

* Due to absence of bS20c sequence information in the publicly available databases, sequence information was extracted by performing BLAST search against the spinach genome (<http://bvseq.molgen.mpg.de>) (12).

Supplementary Table S4. Components of the intersubunit bridges in spinach chloroplast 70S ribosome

Bridge	SSU component	LSU component	Type
B1a	uS13c: Ile111, Glu112, Arg113	23S: H38 (A-site finger): 896-900	R-P
B1b	uS13c: Ile37	uL5c: Arg163, Thr164	P-P
	uS13c: Glu96, Val97	uL5c: Arg165, Asp166	P-P
	uS13c: Arg113	bL31c: C-terminal*	P-P
B1c	uS14c: Asp39, Lys40	bL31c: C-terminal*	P-P
	uS19c: Pro9, Pro42	bL31c: C-terminal*	P-P
	16S: h42 (A1259, G1260)	bL31c: C-terminal*	R-P
B2a/d	16S: h44 (U1444)	23S: H69 (A1926)	R-R
	16S: h44 (C1445)	23S: H69 (C1934)	R-R
	16S: h44 (C1356, A1357)	23S: H69 (A1932, A1933)	R-R
	16S: h45 (G1466)	23S: H69 (A1933)	R-R
	16S: h24 (739)	23S: H69 (G1935, G1936)	R-R
B2b	16S: h24 (G732)	23S: H68 (C1846, C1847)	R-R
B2c	16S: h27 (C848, A849)	23S: G1841, C1842	R-R
B3	16S: h44 (C1369, U1370, G1371, G1372)	uL14c: Pro48, Asn49, Arg54	R-P
	16S: h44 (G1431, A1432, C1433, G1366, A1367, G1368)	23S: H71 (C1961, G1962, G1963, C1972, G1973, A1974)	R-R
B4	uS15c: Ile33, Thr37, Leu40, Glu41, Gln50, Leu53, Arg54, Leu57	23S: H34 (U725, G726, A727)	R-P
	16S: h20 (G710)	23S: H34 (A729)	R-R
B5	16S: h44 (U1376, G1377, C1378, A1422, G1423, G1424)	23S: H62 (C1722, G1723, A1725, A1737, G1738, G1739, G1740)	R-R
B6	16S: h44 (C1380, G1381)	bL19c: Arg228	R-P

B7a	16S: h23 (A650)	23S: H68 (G1856, A1857, A1858, C1908, C1909)	R-R
B7b	Not observed in our cryo-EM reconstruction		
B7c	bS6c: Lys161**, Ala162**	uL2c: Pro132, Leu133, Ala162, Lys163	P-P
B8	16S: h14 (A315, C316, G317)	bL19c: Lys159, Arg160	R-P
	16S: h14 (G308, A309)	uL14c: Arg97	R-P

Abbreviations: R-R=RNA-RNA, R-P=RNA-protein, P-P=Protein-protein

SUPPLEMENTARY REFERENCES

1. Kucukelbir, A., Sigworth, F.J. and Tagare, H.D. (2014) Quantifying the local resolution of cryo-EM density maps. *Nat Methods*, **11**, 63-65.
2. Rosenthal, P.B. and Henderson, R. (2003) Optimal Determination of Particle Orientation, Absolute Hand, and Contrast Loss in Single-particle Electron Cryomicroscopy. *Journal of Molecular Biology*, **333**, 721-745.
3. Bell, J.M., Chen, M., Baldwin, P.R. and Ludtke, S.J. (2016) High resolution single particle refinement in EMAN2.1. *Methods*, **100**, 25-34.
4. Scheres, S.H. (2012) RELION: implementation of a Bayesian approach to cryo-EM structure determination. *J Struct Biol*, **180**, 519-530.
5. Ahmed, T., Yin, Z. and Bhushan, S. (2016) Cryo-EM structure of the large subunit of the spinach chloroplast ribosome. *Sci Rep*, **6**, 35793.
6. Noeske, J., Wasserman, M.R., Terry, D.S., Altman, R.B., Blanchard, S.C. and Cate, J.H.D. (2015) High-resolution structure of the Escherichia coli ribosome. *Nat Struct Mol Biol*, **22**, 336-341.
7. Greber, B.J., Bieri, P., Leibundgut, M., Leitner, A., Aebersold, R., Boehringer, D. and Ban, N. (2015) Ribosome. The complete structure of the 55S mammalian mitochondrial ribosome. *Science*, **348**, 303-308.
8. Jenner, L.B., Demeshkina, N., Yusupova, G. and Yusupov, M. (2010) Structural aspects of messenger RNA reading frame maintenance by the ribosome. *Nat Struct Mol Biol*, **17**, 555-560.
9. Polikanov, Y.S., Melnikov, S.V., Soll, D. and Steitz, T.A. (2015) Structural insights into the role of rRNA modifications in protein synthesis and ribosome assembly. *Nat Struct Mol Biol*, **22**, 342-344.
10. Rice, P., Longden, I. and Bleasby, A. (2000) EMBOSS: the European Molecular Biology Open Software Suite. *Trends Genet*, **16**, 276-277.
11. Ban, N., Beckmann, R., Cate, J.H., Dinman, J.D., Dragon, F., Ellis, S.R., Lafontaine, D.L., Lindahl, L., Liljas, A., Lipton, J.M. *et al.* (2014) A new system for naming ribosomal proteins. *Curr Opin Struct Biol*, **24**, 165-169.
12. Dohm, J.C., Minoche, A.E., Holtgrawe, D., Capella-Gutierrez, S., Zakrzewski, F., Tafer, H., Rupp, O., Sorensen, T.R., Stracke, R., Reinhardt, R. *et al.* (2014) The genome of the recently domesticated crop plant sugar beet (*Beta vulgaris*). *Nature*, **505**, 546-549.

Figure S1

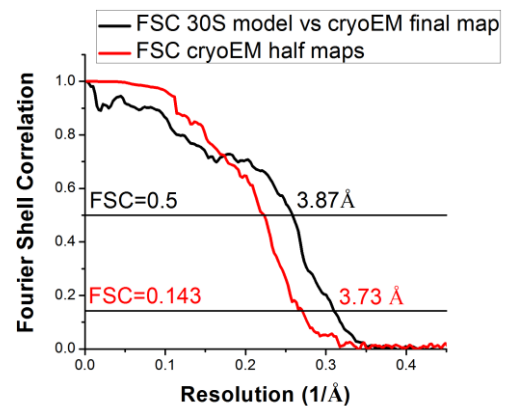
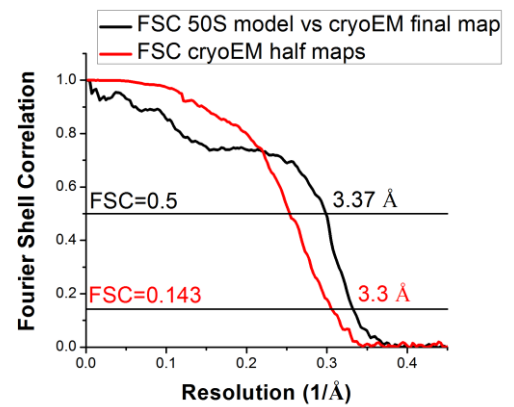
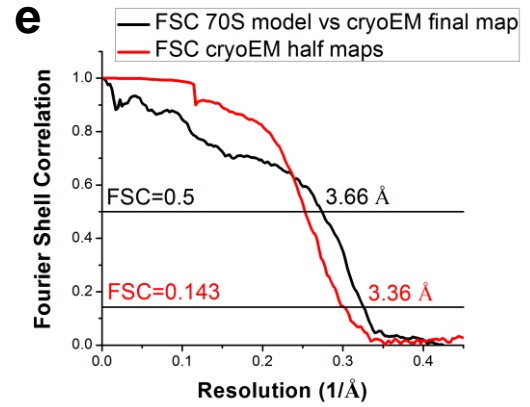
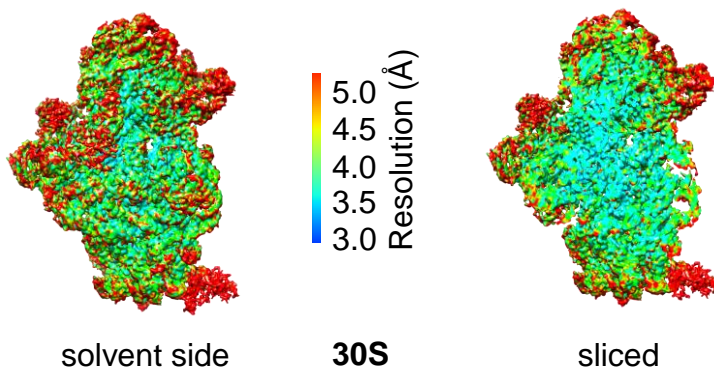
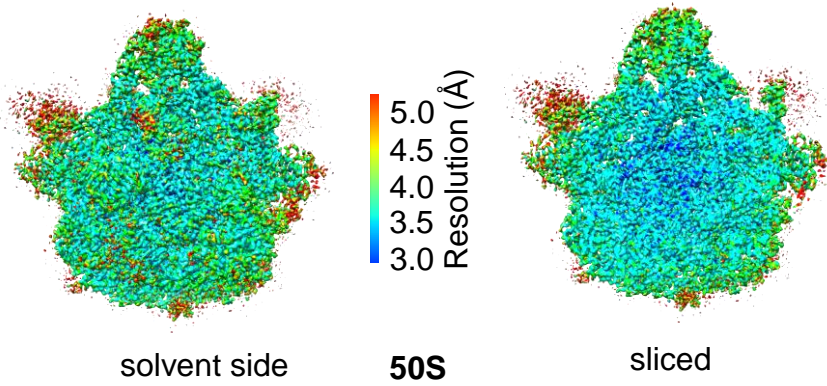
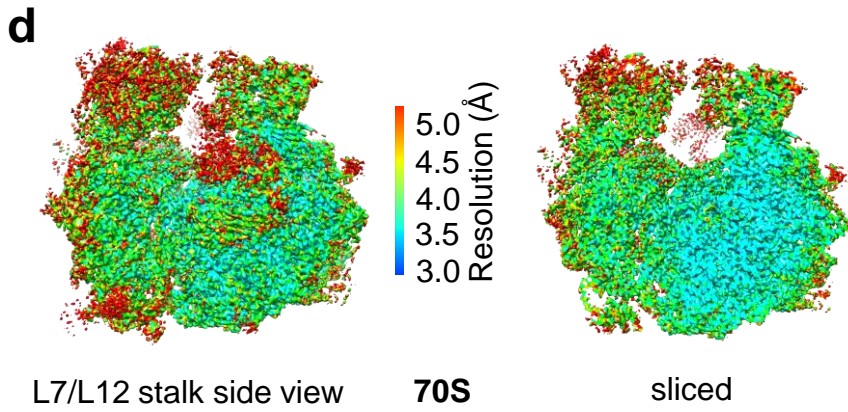
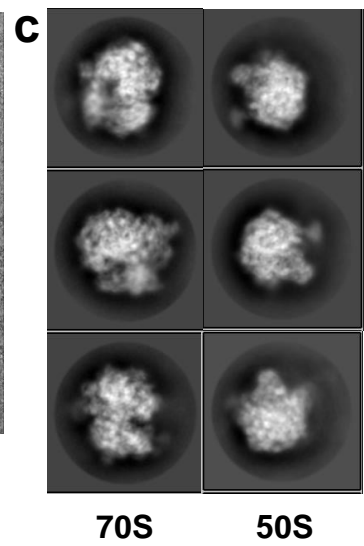
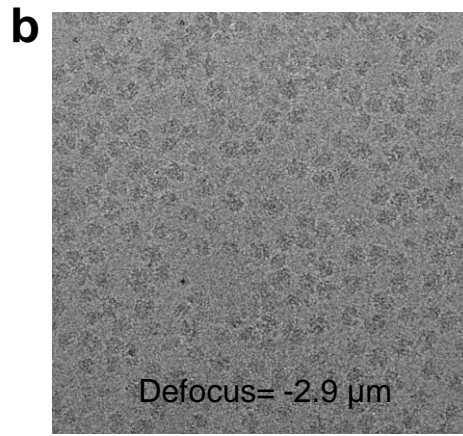
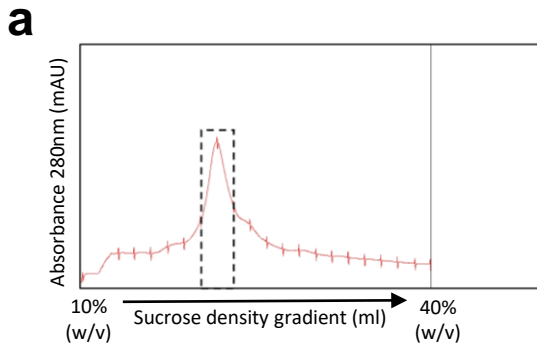
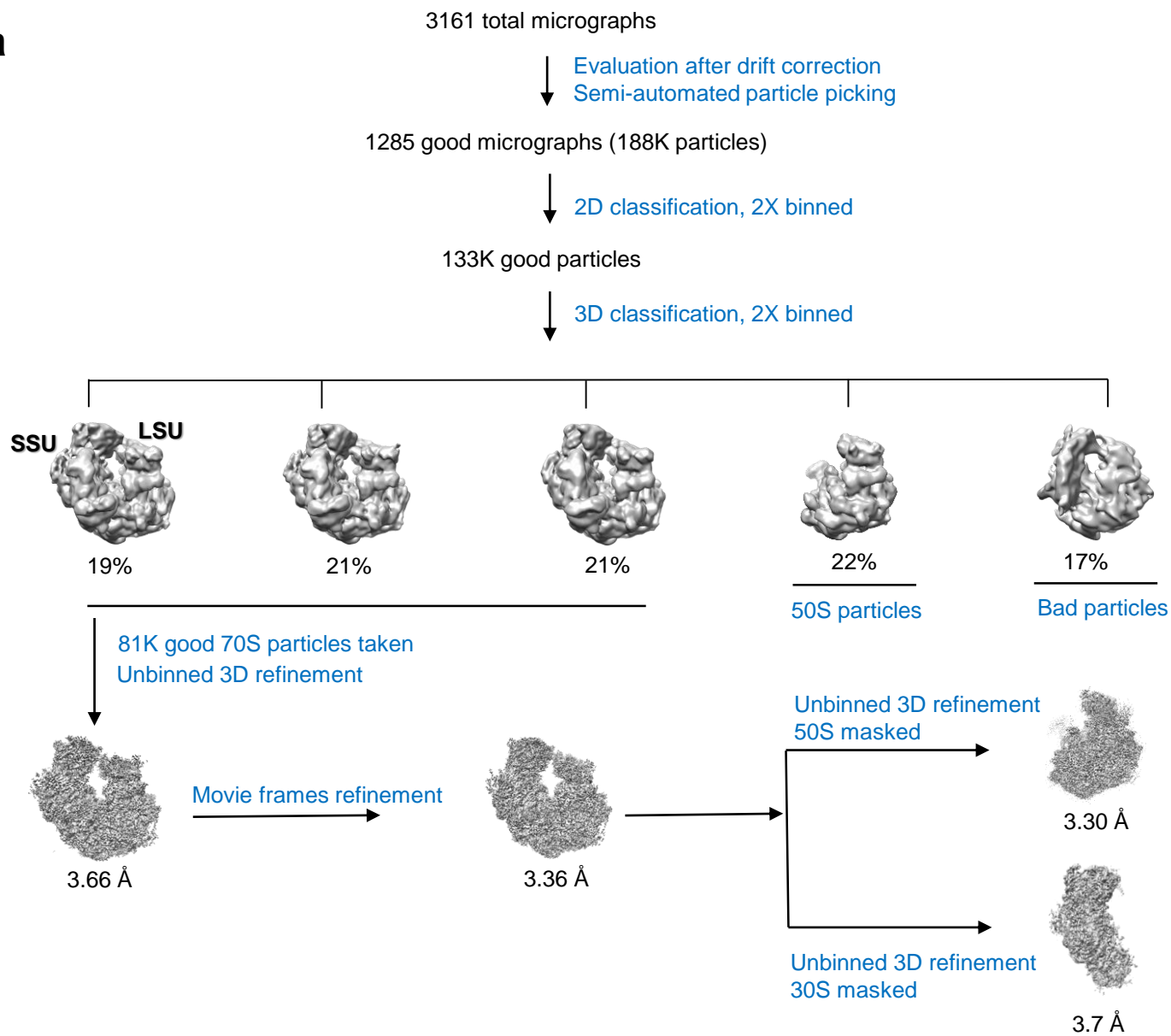


Figure S2

a



b

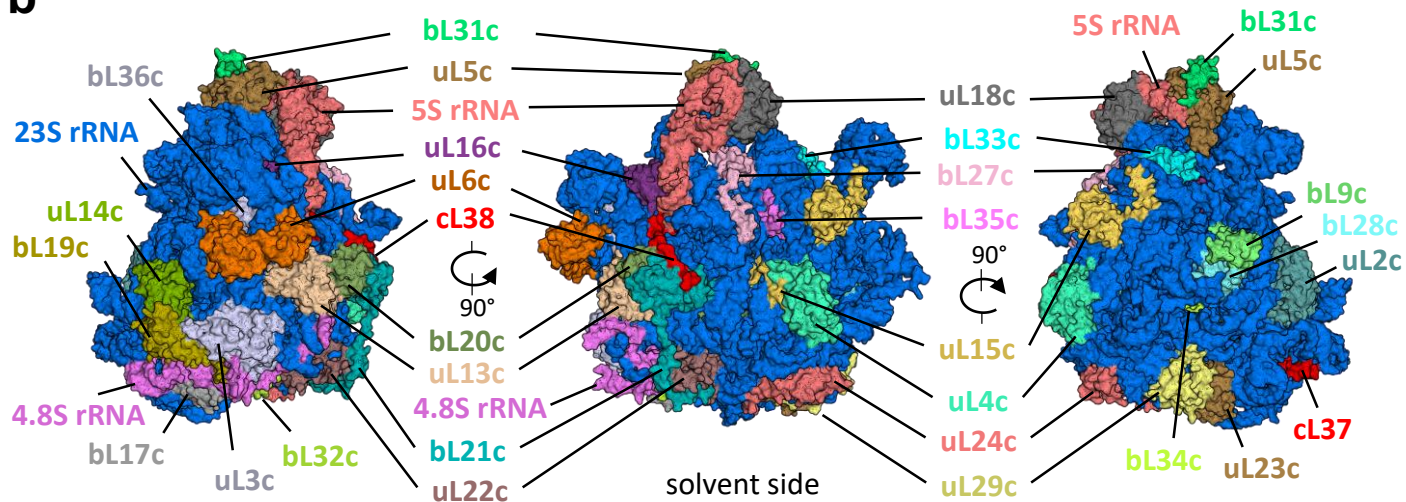
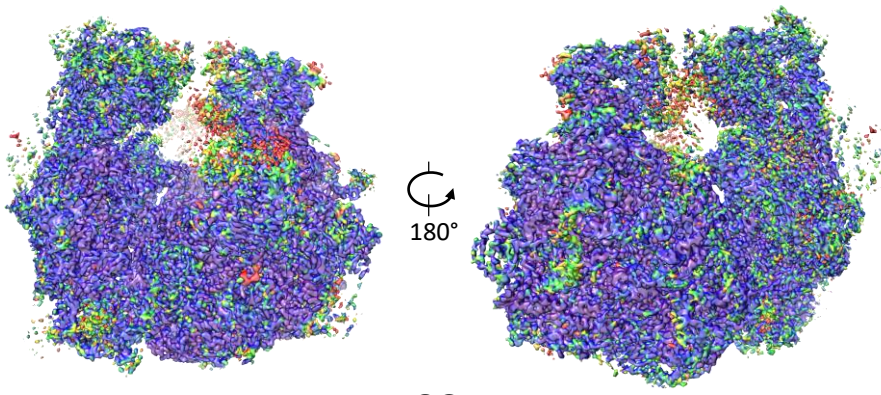


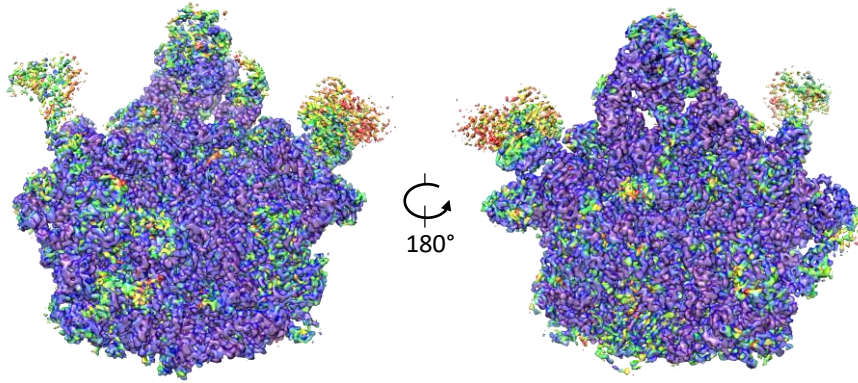
Figure S3



L7/L12 stalk side

70S

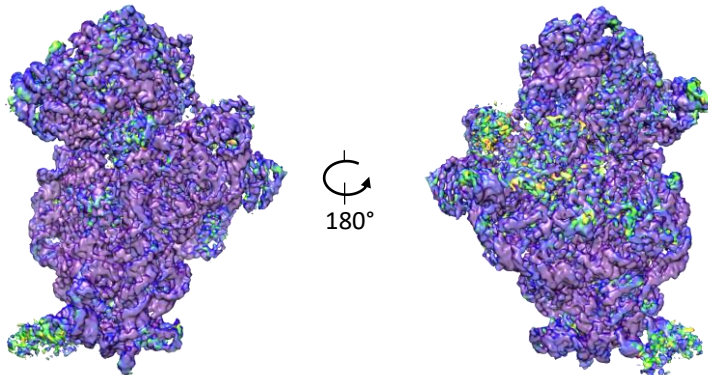
L1 stalk side



intersubunit side

50S

solvent side



intersubunit side

30S

solvent side

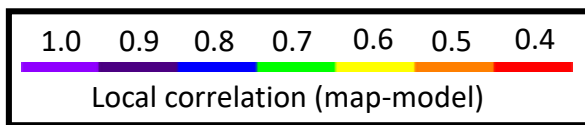


Figure S4

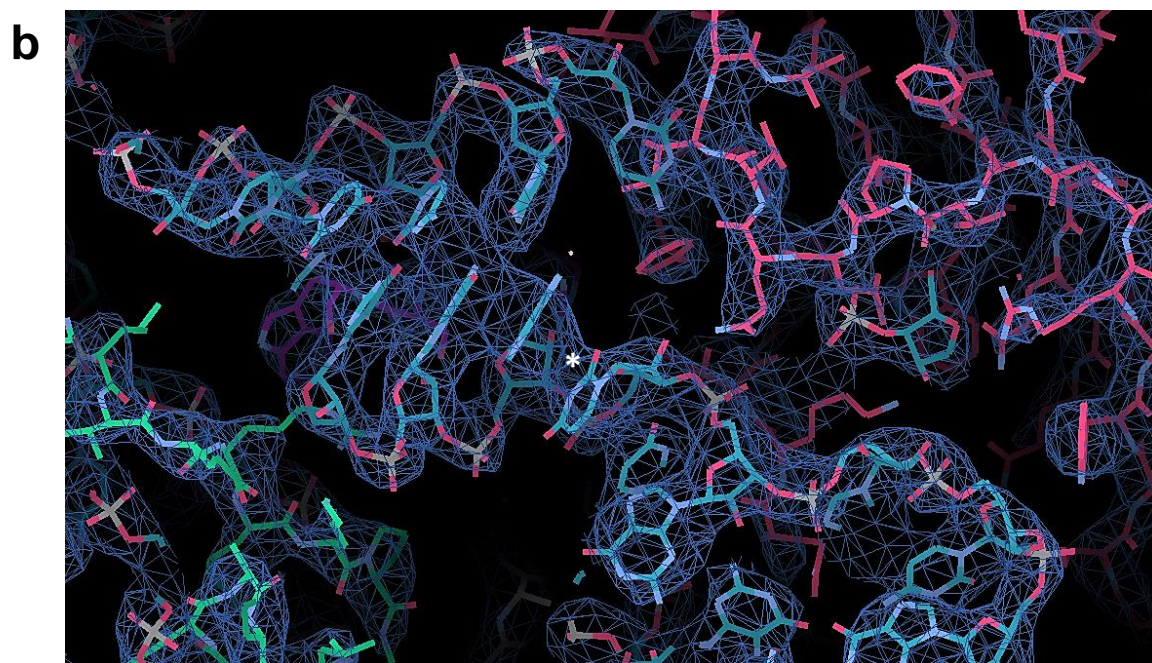
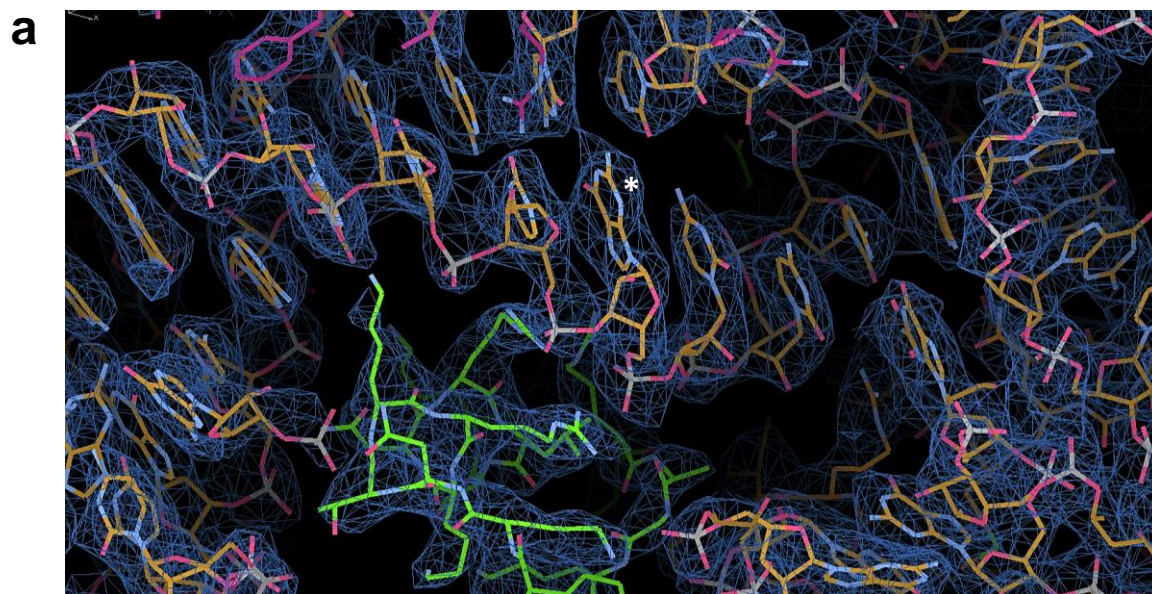


Figure S5

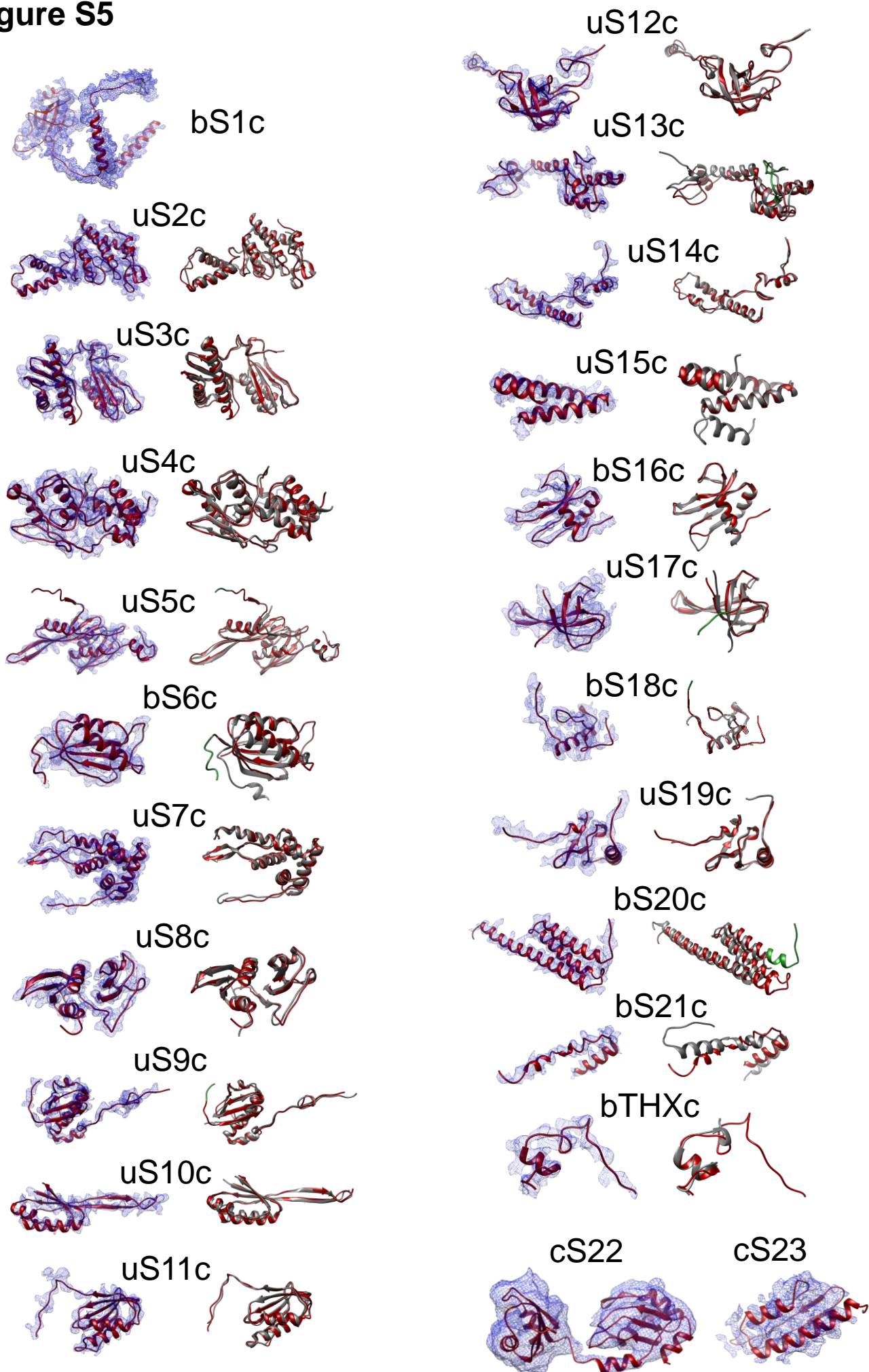
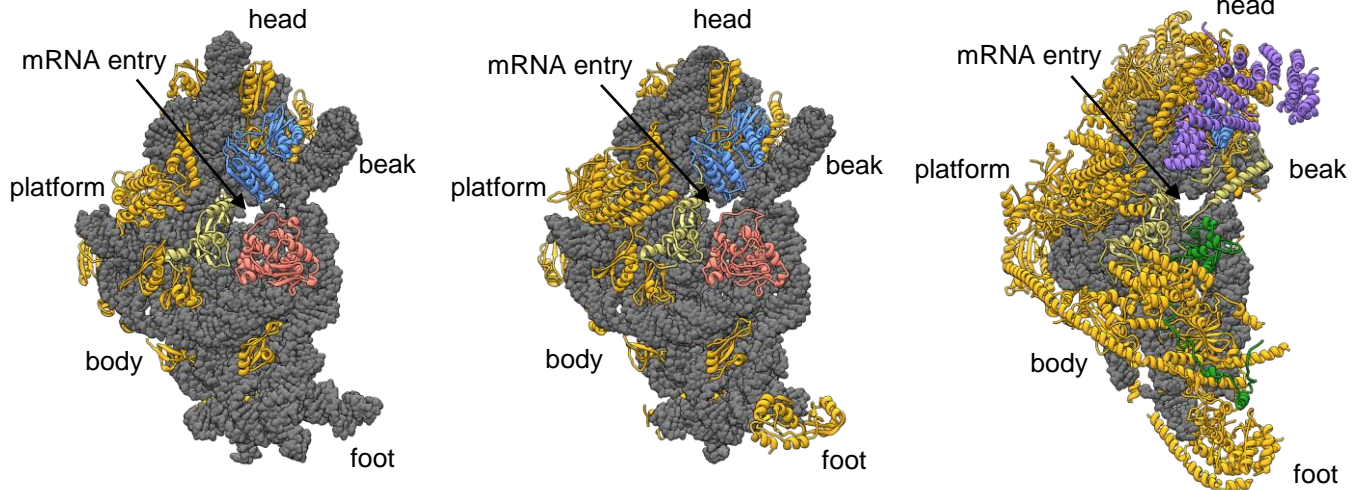


Figure S6

a



b

bacterial 30S chloroplast 30S mitochondrial 30S

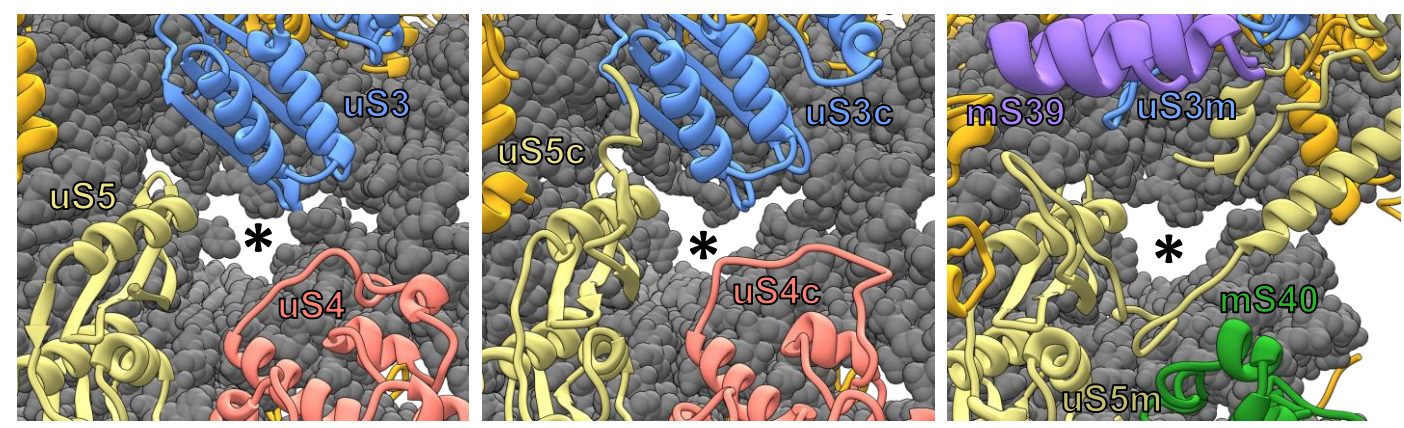
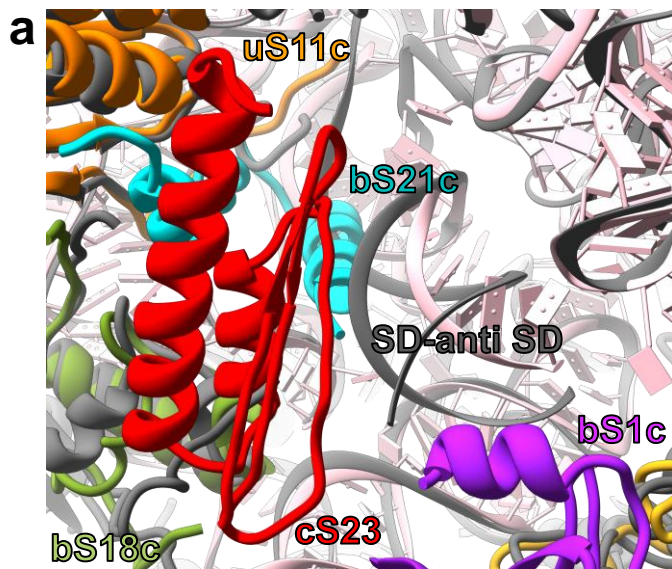
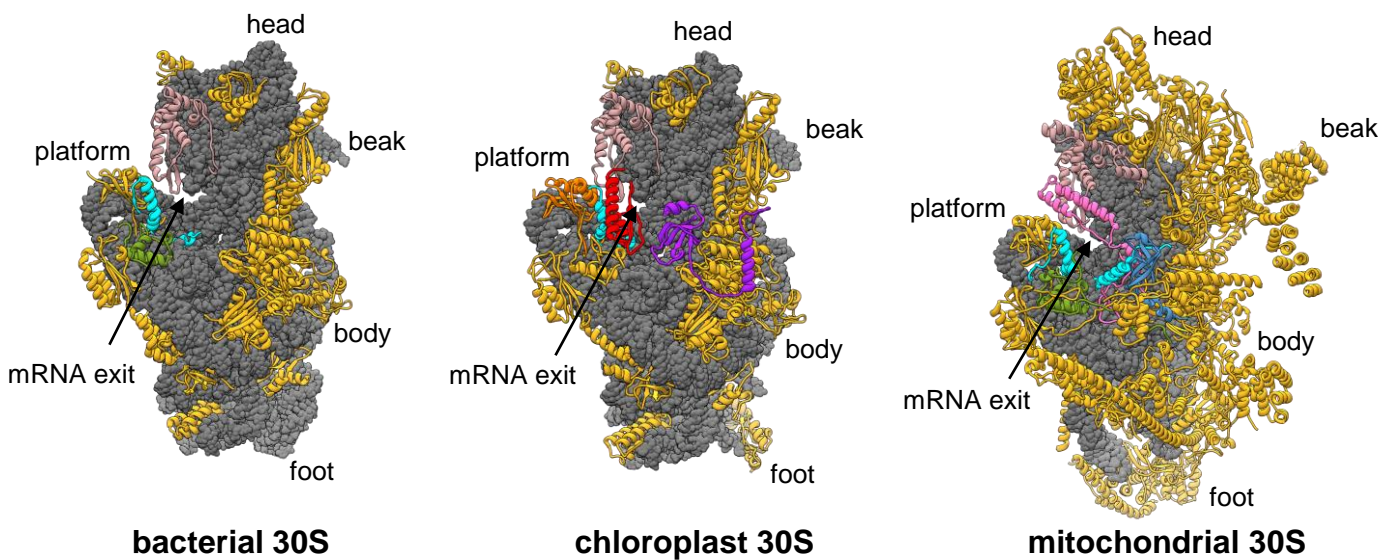


Figure S7



b



c

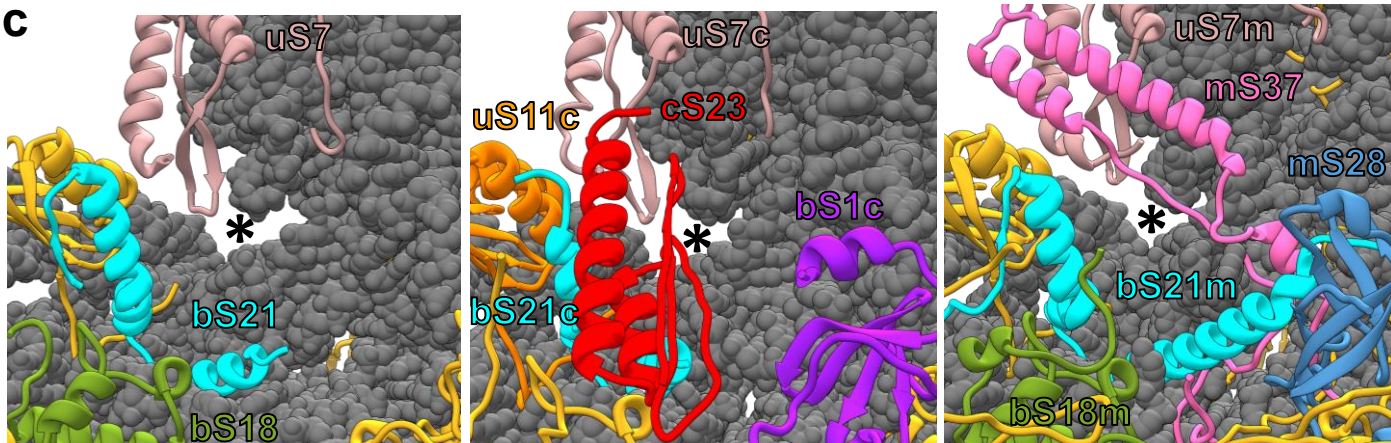


Figure S9

